Journal of Molecular Graphics and Modelling 49 (2014) 80–90

Contents lists available at ScienceDirect

Journal of Molecular Graphics and Modelling

journal homepage: www.elsevier.com/locate/JMGM

Characterization of CO_2 and mixed methane/CO_2 hydrates intercalated in smectites by means of atomistic calculations

Rubén Martos-Villa [a,*], M. Pilar Mata [b], C. Ignacio Sainz-Díaz [c]

[a] Facultad de Ciencias del Mar y Ambientales, Universidad de Cádiz, Av. República Saharaui s/n, 11510 Puerto Real, Spain
[b] Instituto Geológico y Minero de España, La Calera 1, 28760, Tres Cantos, Madrid, Spain
[c] Instituto Andaluz de Ciencias de la Tierra, CSIC-Universidad de Granada, Av. de las Palmeras, 4, 18100, Armilla, Granada, Spain

ARTICLE INFO

Article history:
Received 2 October 2013
Received in revised form 2 January 2014
Accepted 27 January 2014
Available online 3 February 2014

Keywords:
Gas hydrates
CO_2 clathrates
CO_2 sequestration
Smectites
Molecular Dynamics
Methane hydrate

ABSTRACT

The recent increase in anthropogenic CO_2 gas released to the atmosphere and its contribution to global warming make necessary to investigate new ways of CO_2 storage. Injecting CO_2 into subsurface CH_4 hydrate reservoirs would displace some of the CH_4 in the hydrate crystal lattice, converting simple CH_4 hydrates into either simple CO_2 hydrates or mixed CH_4—CO_2 hydrates. Molecular simulations were performed to determine the structure and behavior of CO_2 and mixed hydrate complexes in the interlayer of Na-rich montmorillonite and beidellite smectite. Molecular Dynamics (MD) simulations used NPT ensembles in a $4 \times 4 \times 1$ supercell comprised of montmorillonite or beidellite with CO_2 or mixed CH_4/CO_2 hydrate complexes in the interlayer. The smectite 2:1 layer surface helps provide a stabilizing influence on the formation of gas hydrate complexes. The type of smectite affects the stability of the smectite-hydrate complexes, where high charge located on the tetrahedral layer of the smectites disfavor the formation of hydrate complexes.

1. Introduction

Natural gas hydrates (NGH) are crystalline compounds consisting of methane molecules encaged in cavities of a hydrogen-bonded network of water molecules. These clathrates present cubic sI structure that consists of 46 water molecules per unit cell, forming two dodecahedron (5^{12}) and six tetradecahedron ($5^{12}6^2$) cages. Considerable amounts of methane hydrate can be found in permafrost regions and sediments of the ocean floor in outer continental margin regions [1–3], where medium pressures, low temperatures and high methane gas concentration in water can be reached [4–7].

Natural gas hydrates are seen as a potential major energy resource and recently new techniques has been developed to enable an economical extraction of these complex deposits [8]. However, some environmental issues need to be taken in account. Methane is a powerful greenhouse gas, so the large scale destabilization of hydrates would cause great impact on Earth's climate, dramatically increasing the temperature of the planet [9].

The recent increase in anthropogenic CO_2 gas released to the atmosphere and its contribution to global warming, makes necessary to investigate new ways of CO_2 storage. It has been suggested that CO_2 can be stored as a solid in the form of clathrate hydrates or as a pool of liquid bellow a cap of its hydrate [10]. The possibility of replacing natural gas by CO_2 from NGH has been investigated improving the economic viability of CO_2 storage [11–13]. There are thermodynamic evidences that support the replacement in hydrate at appropriate conditions. The comparison of their hydrate phase equilibrium conditions suggests the occurrence of a transition zone between both hydrate equilibrium curves where CO_2 hydrates can exist while CH_4 hydrates dissociate into methane gas and water [14]. In addition, the heat of formation of carbon dioxide hydrate (−57.98 kJ/mol) is greater than the heat of dissociation of methane hydrate (54.49 kJ/mol). The heat released from the formation of carbon dioxide hydrate in the presence of methane hydrate should be sufficient to dissociate the methane hydrate and recover methane gas [15]. Furthermore, it has been experimentally proven that carbon dioxide is preferentially trapped over methane in the hydrate phase [16]. These observations fuel the growing interest in the use of carbon dioxide for natural gas recovery from gas hydrate deposits. Any further investigation of the mixed CO_2–CH_4 gas hydrate properties could lead to major breakthroughs in the fields of unconventional resource production and carbon sequestration.

A better understanding of the molecular mechanism leading to hydrate crystallization and decomposition is a crucial part of the practical problems mentioned above. Experimental studies of clathrates are complex by the working handicaps in conditions of stability of these compounds, and it is difficult to obtain sufficient

* Corresponding author. Tel.: +34 607843397.
E-mail addresses: ruben.martos@uca.es, r_marxs@hotmail.com (R. Martos-Villa).

1093-3263/$ – see front matter © 2014 Elsevier Inc. All rights reserved.
http://dx.doi.org/10.1016/j.jmgm.2014.01.008

reliable data. On the other hand, theoretical studies of Computational Mineralogy can be very useful to understand and interpret experimental results.

Studies of Monte Carlo (MC) and Molecular Dynamics (MD) calculations on the structural and thermodynamic properties of methane hydrates have been reported. Radhakrishnan and Trout [17] and Ota and Ferdows [18] studied the formation process and thermodynamic properties of CO_2 hydrates respectively using MC method. MD techniques has been used with different force fields to calculate physical–chemical properties [19] and to describe different properties of methane hydrates like mechanism of nucleation and crystal growth kinetics [20,21]; decomposition mechanism [22,23]; and replacement of methane hydrate by CO_2 [24,25].

In recent years the study of gas storage as hydrate in depleted gas reservoir is growing. In a gas-hydrate bearing marine sediments, smectite, has been described so far, as an abundant clay mineral [26]. Clay minerals sorb considerable amounts of methane [27]. Swelling clays such as montmorillonite and beidellite usually contains multiples planes of weakly bonded H_2O in the interlayer between the 2:1 (silicate) layers. Because of the weakness of the atomic forces between H_2O and the 2:1 layer, together with the knowledge that interlayer area is about 90% of mineral surface, most of adsorption processes will take place on this interlayer space. Guggenheim and Koster van Groos [28] succeeded in intercalating methane hydrate and the 2:1 layers of Na-exchanged montmorillonite.

On the other hand, the challenge of injecting CO_2 into sedimentary rocks is to predict the long-term behavior of the impermeable cap rock sealing the reservoir against leakage of the injected CO_2 [29,30]. This cap-rock is generally a shale or mudstone rich in clay minerals, often including swelling clays. CO_2 exposure can significantly affect the structure of smectite. Swelling clay particle could expand due to the incorporation of CO_2 directly, or it could dehydrate and contract if the supercritical CO_2 has a greater affinity for water molecules than the clay [31].

Because of the limited experimental data and analysis of natural samples, in this work molecular modeling has been used to obtain information about possible ways to incorporate CO_2 in smectites. The study of the behavior and interactions of CO_2 and CH_4—CO_2 hydrates in an expanded clay structure at atomistic level by molecular simulations is the main objective of this work. Theoretical data can show how subtle differences on type of clays, like tetrahedral charge can favor or disfavor the formation of hydrate in the interlayer space. Molecular simulations are also useful to describe the structure and behavior at atomistic level of these new compounds formed by hydrates intercalated on smectites.

2. Computational methodology

Ab initio total energy calculations of the periodic crystal model of hydrates were performed using Density Functional Theory (DFT) methods implemented in the SIESTA program [32]. We used the generalized gradient approximation (GGA) with the Perdew–Burke–Ernzerhof (PBE) and revised PBE functional (RPBE) of the exchange–correlation functional [33]. Core electrons were replaced by norm-conserving pseudopotentials [34] in the SIESTA calculations. Pseudopotentials simulate the interaction between valence electrons and cores (nuclei plus core electrons) and neither core electrons nor core wave functions have to be included explicitly. With this approximation the valence wave functions are substituted by pseudo-wave functions that do not present strong oscillations in the core region. Calculations were restricted to the Γ point in the irreducible wedge of the Brillouin zone. In all structures, all atoms were relaxed by means of conjugated gradient minimizations at constant volume. In SIESTA, the basis sets are made with strictly localized numerical atomic orbitals (NAOs) with a localization cut-off radii corresponding to an energy shift of 270 meV. These basis sets used in this work are double-Z polarized (DZP) following the perturbative polarization scheme. This method has been used successfully for modeling of phyllosilicates previously [35,36]. For the H and O atoms, we used bases and pseudopotentials both optimized by Fernández-Serra and Artacho [37].

It is known that, in some cases, quantum mechanical methods do not describe well enough the dispersive interactions and weak adsorption interactions. Many empirical corrections and new functionals have been developed and still are developing in order to describe better these weak interactions. However, recent benchmark studies [38,39] have shown that there is no dispersion correction yet, which describe properly systems like our clathrates with a mixture of electrostatic, van der Waals and H bonding interactions. Hence, empirical interatomic potentials were also used in order to overcome these discrepancies. These empirical potentials were used within a Force Field (FF) that has recently been optimized by Heinz et al. [40] based on CVFF (consistent valence force field) that has been named CVFFH. These FF have yielded good results in phyllosilicates with organics [41]. The atomic charges were taken from charges calculated at the ab initio MP2/6-311G** level and associated with the electrostatic field (ESP) with the method of Merz and Kollman [42] for the methane molecule. Different calculation conditions were tuned with respect to the 12–6 (CVFF) Lennard–Jones potentials and with van der Waals and Coulomb interactions. The van der Waals atom based interactions with a cut-off of 15.5 Å and the Ewald summation for Coulomb interactions yielded the best results and these conditions were used in this work. Molecular dynamic simulations were performed with this force field with several ensembles and steps of 1 fs. The temperature and pressure of the model system were controlled using Andersen [43] and Berendsen [44] methods, respectively. For these CVFFH calculations, we employed periodical boundary conditions for crystal lattice structures with the Discover program within the Material Studio package [45].

The Molecular Dynamics simulations have been performed with the CVFF approximation within the NPT ensemble (at constant temperature and pressure and variable volume) with steps of 1 fs.

The adsorption energy was calculated as follows:

$$U_{\text{adsorption}} = U_{\text{complete hydrate structure}} - (U_{\text{empty hydrate (no guest molecules}} + nU_{\text{guest molecules}}),$$

where U is the internal energy of the each system fully optimized at constant volume, and the guest molecules are CO_2 or CH_4, and were calculated isolated in an empty cell with the same size of the hydrates crystal lattice. Only complete occupancy was considered. Then, in the CO_2 clathrate crystal, there are $8CO_2$ molecules per unit cell, and in the mixed CH_4/CO_2 clathrate crystal there are $2CH_4$ and $6CO_2$ molecules per unit cell. In the cases with smectite the adsorption energy was:

$$U_{\text{adsorption}} = U_{\text{smectite-gas hydrate intercalate}} - (U_{\text{gas hydrate}} + U_{\text{smectite}}).$$

3. Models

Montmorillonite and beidellite are dioctahedral phyllosilicates, where each 2:1 layer is formed by two sheets composed of tetrahedrally coordinated Si atoms (with four oxygen atoms) and a central sheet formed by octahedrally coordinated Al atoms (with six oxygen atoms neighbors). For montmorillonite, layer charge is created primarily by substitution of divalent metals (e.g., Mg^{2+} and Fe^{2+}) for the Al^{3+} in the octahedral sheet. However, for beidellite, layer charge is obtained by substitution of Al^{3+} for the Si^{4+} in the tetrahedral sheet. In both cases, the negative layer charge is balanced by

interlayer exchangeable cations (e.g., Na^+, K^+, Ca^{2+}), that are easily hydrated by ambient water molecules.

Montmorillonite and beidellite models were based on previous pyrophyllite models [46]. Pyrophyllite is a dioctahedral 2:1 phyllosilicate [47] with similar structure to montmorillonite and beidellite, but without substitutions and no layer charge. A $4 \times 4 \times 1$ supercell was created. For the montmorillonite model, ten Al^{3+} are replaced by Mg^{2+} and layer charge is balanced by ten tetrahedrally hydrated Na^+ cations in the interlayer, resulting in a simulation cell composition of $Na_{10}(Si_{128})(Al_{54}Mg_{10})O_{320}(OH)_{64}.40H_2O$. The beidellite model was created by replacing ten tetrahedrally coordinated Si^{4+} by Al^{3+} (five in each tetrahedral sheet), balancing the charge with ten tetrahedrally hydrated Na^+ interlayer cations. This represents an hydration level of 2.5 water molecules per unit cell of clay. The beidellite simulation cell has a composition of $Na_{10}(Si_{118}Al_{10})(Al_{64})O_{320}(OH)_{64}.40H_2O$. In both cases, maximum dispersion of the substituted cations in the tetrahedral and octahedral sheets were made according to previous studies [48,49]. Initial lattice parameters of each $4 \times 4 \times 1$ smectite supercell are $a = 20.64$ Å, $b = 35.86$ Å, $c = 12.34$ Å; $\alpha = 88°$, $\beta = 103°$, $\gamma = 90°$. For smectite-hydrate intercalate models, the c-axis value was set at 30 Å to create sufficient space to introduce unit cells of methane hydrate.

Hydrate models were derived from experimental crystallographic data [50]. In case of CO_2 hydrates, a unit cell was generated including 178 atoms with 46 water molecules and $8CO_2$ molecules, with lattice parameters of $a = b = c = 11.97$ Å; $\alpha = \beta = \gamma = 90°$ (Fig. 1a). For mixed CH_4—CO_2 hydrates, basing on previous calculations [51] CO_2 molecules were placed on large $5^{12}6^2$ cages, and CH_4 molecules were placed in small 5^{12} cages (Fig. 1b). This arrangement is because adsorption energy of CO_2 molecule in the large cage is more exothermic than in the small one. Larger simulation cells required for the bulk hydrate structure were created by expanding the unit cell in integral units.

For smectites-gas hydrates intercalate simulations, a $3 \times 3 \times 1$ methane hydrate supercell (414 water molecules + 72 gas molecules) was created. This supercell was cut to fit with the smectite a–b crystallographic dimensions (20.64×35.86 Å) to the smectite supercell model. Thus, the hydrate fits into the smectite interlayer space without losing periodic boundary conditions.

4. Results and discussion

Previous experimental results proved that a smectite-methane hydrate complex can be formed for Na-exchanged montmorillonite and Na-exchanged nontronite [28,52]. We consider the Na-exchanged montmorillonite and hydrate complexes given by Guggenheim and Koster van Groos (2003) [28].

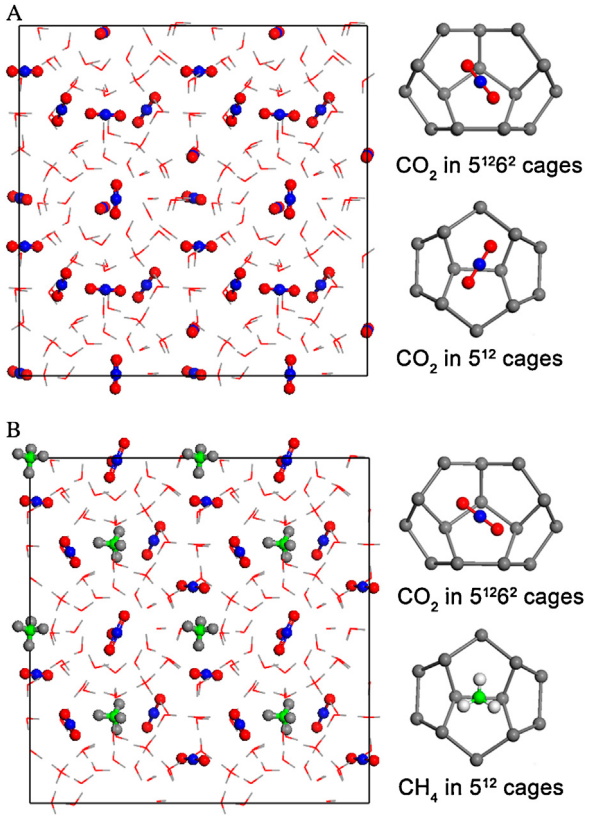

Fig. 1. Schematic framework of cages extracted from the crystal lattice of CO_2 (a) and mixed (b) hydrates. Red and gray lines represent O and H atoms from water molecules. Blue and red balls represent C and O atoms from carbon dioxide molecules; green and gray balls represent C and O atoms from methane molecules.

4.1. CO_2 and CH_4—CO_2 mixed hydrates crystal structure

Geometry optimization calculations for one unit cell of a CO_2 and a CH_4—CO_2 mixed hydrate model (structure SI) were performed at constant and variable volume. All atoms positions were optimized, applying different simulation methods: based on DFT (SIESTA), and based on empirical interatomic potentials (CVFFH). In CVFFH calculations, the SPC model for water molecules was applied. For the crystal structures optimized at variable volume with the different methods described above, lattice parameters of calculated hydrate unit cell have been compared (Table 1). Our calculated lattice values are close to the experimental ones [53] and the crystal structure of CO_2 hydrates can be successfully reproduced using these methods. Nevertheless, it can be noticed that the closest values to experimental are obtained with SIESTA and PBE parameterization, whereas

Table 1
Crystal lattice parameters of CO_2 and mixed CH_4—CO_2 hydrates fully optimized at variable volume by different theoretical methods and comparison with experimental data (distances in Å and angles in°).

Features	Methods	a (Å)	b (Å)	c (Å)	α (°)	β (°)	γ (°)
CO_2 Hydrates	Exp[a]	11.89	11.89	11.89	90	90	90
	GGA/PBE[b]	11.92	11.75	11.76	90.8	92.2	88.3
	GGA/RPBE[c]	12.41	12.32	12.37	90.6	91.9	88.1
	CVFFH[d]	11.78	11.39	11.43	88.9	91.3	93.6
CH_4—CO_2 mixed hydrates	GGA/PBE[b]	11.91	11.69	11.64	89.9	89.8	90.2
	GGA/RPBE[c]	12.23	12.24	12.18	90.4	90.5	89.5
	CVFFH[d]	11.64	11.33	11.57	88.5	89.5	91.8

[a] From experimental structure of CO_2 hydrates obtained from X-ray diffraction (Udachin et al., 2001 [53]).
[b] Optimized with SIESTA and PBE parameterization.
[c] Optimized with SIESTA and RPBE parameterization.
[d] Calculated with CVFFH force field and SPC model for water molecules.

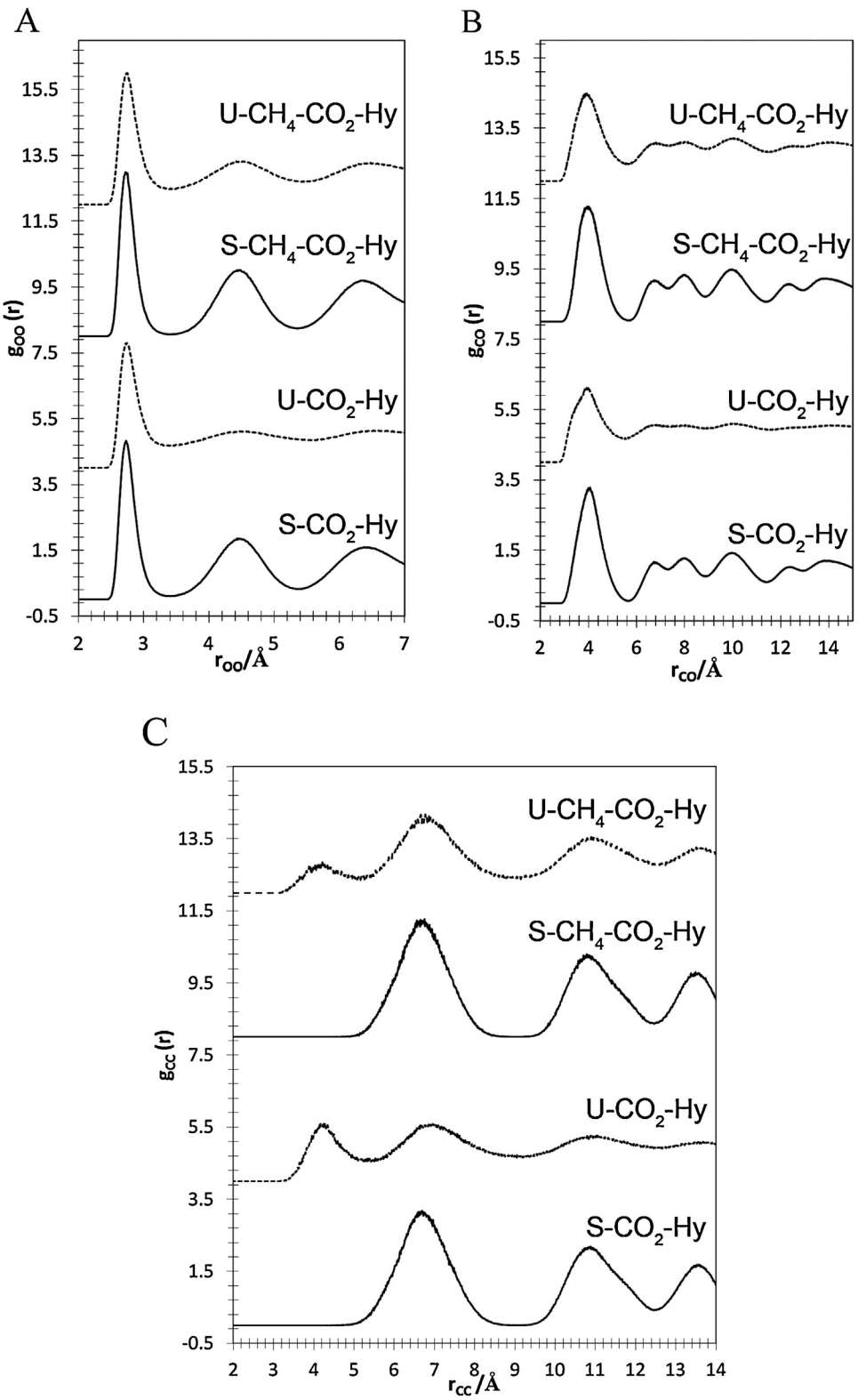

Fig. 2. RDFs of OO (a), CO (b) and CC (c) atoms of the crystal lattice of CO_2 and mixed CH_4—CO_2 hydrate (Hy) simulated by MD at 40 bar and 273 K (S-CO_2-Hy and S-CH_4-CO_2-Hy) and 40 bar and 320 K (U-CO_2-Hy and U-CH_4-CO_2-Hy).

the RPBE parameterization approximation tends to make lattice parameters larger than experimental. In spite of the lack of dispersion correction, the GGA/PBE calculations.

Adsorption energies of gas molecules into the clathrate crystal were calculated. Calculations with CVFFH yield −40.34 kcal/mol per unit cell for CO_2 hydrates, while for mixed CH_4—CO_2 hydrates the adsorption energy is more negative, being −41.91 kcal/mol per unit cell.

MD simulations of a $2 \times 2 \times 2$ supercell of fully occupied CO_2 hydrate and CH_4—CO_2 mixed hydrate were performed for 100 ps

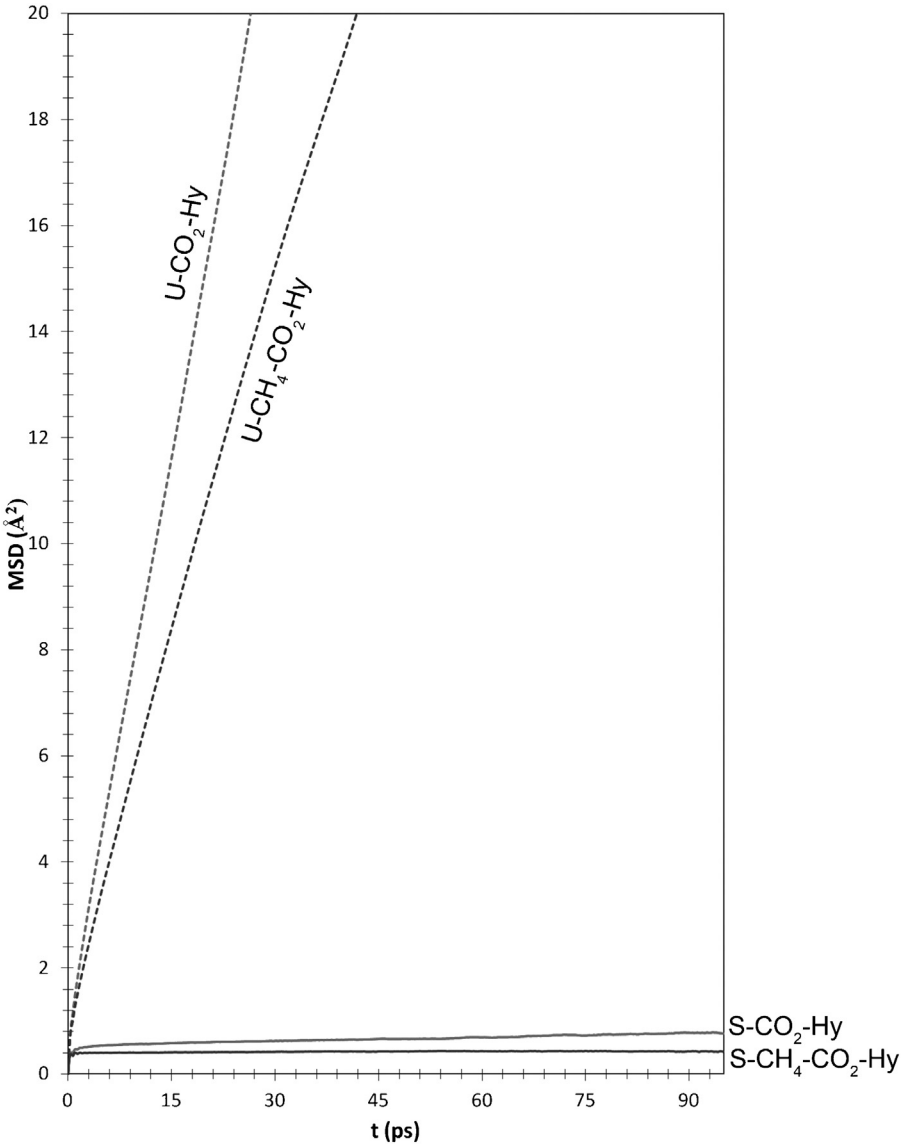

Fig. 3. MSD of water molecules in CH_4—CO_2 and CO_2 hydrates obtained from MD simulations.

at two different conditions: Under stable conditions at pressure $P = 40$ bar and temperature $T = 273$ K (S-CO_2-Hy and S-CH_4-CO_2-Hy) and in unstable conditions at $P = 40$ bar and $T = 320$ K (U-CO_2-Hy and U-CH_4-CO_2-Hy). The Radial Distribution Function (RDF) is a measure of the average distances (r) between pairs of atoms. In this case, RDF are used to compare the structure of hydrates during MD simulations (Fig. 2). RDF profiles were calculated for O–O (distances between oxygen atoms from water molecules); C–O (distance between C atoms of gas molecules and O atoms of water molecules); C–C (distance between C atoms of gas molecules). No difference in these RDF profiles has been observed between S-CO_2-Hy and S-CH_4—CO_2-Hy simulations.

RDF profiles of O–O atom-pairs, g_{O-O}, display a common maximal peak at $r_{O-O} = 2.8$ Å, corresponding to the nearest distance between H_2O molecules linked by hydrogen bonds (Fig. 2a). The second and third maximal peaks appearing in the hydrate model at $r_{O-O} = 4.6$ Å and 6.5 Å respectively, correspond to oxygen coordination in hydrates and they are appear as sharp peaks in the stable conditions (S-CO_2-Hy and S-CH_4-CO_2-Hy), while in the unstable simulations (U-CO_2-Hy and U-CH_4-CO_2-Hy) they are broader and poorly defined. Nevertheless, these peaks are better identified on U-CH_4-CO_2-Hy simulations than in the U-CO_2-Hy. In RDF profiles of C and O atoms, g_{C-O}, a maximal peak at $r_{C-O} = 4$ Å occurs for all MD simulations (Fig. 2b). This peak corresponds to water molecules surrounding the guest molecules. However, the remaining peaks at 6.6 Å, 8.0 Å, and 9.8 Å, which are clearly defined in the stable simulations (S-CO_2-Hy and S-CH_4—CO_2-Hy), are broader and poorly defined in the unstable simulations (U-CO_2-Hy and U-CH_4-CO_2-Hy) due to a slight long-range disorder.

The RDF peaks of C atoms in CH_4 molecules, g_{C-C}, appear at $r_{C-C} = 6.6$ and 10.8 Å (Fig. 2c). The width of these peaks is due to the displacements of the guest molecules into the host cages. These peaks are intense in the stable MD simulations. However, in unstable simulations, these peaks are broader with lower intensity and a new peak can be observed at close C–C distances at 4.0 Å. This indicates that the guest molecules tend to aggregate with rising temperature breaking the crystal lattice structure. Nevertheless, in this C–C profile this effect is smaller in U-CH_4-CO_2-Hy than in U-CO_2-Hy, indicating that the mixed CH_4—CO_2 hydrate crystal structure is more stable than CO_2-Hy.

The mean square displacement (MSD) is a measure of the average distance that a molecule travels during simulations. For a

Table 2
Cell parameters and select interatomic spacings of the CO_2 hydrate (Hy) intercalates in Na-montmorillonite (Mnt) and Na-beidellite (Bei) unit cell (distances in Å and angles in°).

Features	Exp[a]	Na-Mnt[b]	Mnt-CO_2-Hy[b]	S-Mnt-CO_2-Hy[c]	U-Mnt-CO_2-Hy[d]	Na-Bei[b]	Bei-CO_2-Hy[b]	S-Bei-CO_2-Hy[c]	U-Bei-CO_2-Hy[d]
a	5.18	5.16	5.41	5.41	5.41	5.15	5.42	5.42	5.43
b	8.95	8.95	8.92	8.93	8.93	8.92	8.91	8.92	8.93
c	12.34	12.08	23.24	23.25	23.26	12.34	23.06	23.08	23.10
d(0 0 1)	12.13	11.75	22.64	22.64	22.66	11.98	22.26	22.26	22.28
α	90.0	88.0	93.2	93.2	93.2	92.2	95.2	91.2	95.2
β	100.6	103.3	103.1	103.1	103.1	103.8	105.3	105.3	105.3
γ	90.0	90.1	89.3	89.3	89.3	89.4	89.4	89.4	89.4
d(Si–O)	1.65	1.66	1.65	1.65	1.65	1.67	1.65	1.65	1.65
d(Al–O)	1.94	1.94	1.95	1.95	1.95	1.94	1.95	1.95	1.95
d(O–H)		0.93	0.95	0.95	0.95	0.93	0.95	0.95	0.95
d(Na...O_{clay})		2.44	2.40	2.55	2.55	2.35	2.30	2.35	2.35
d(Na...O_w)		2.44	2.45	2.45	2.45	2.44	2.50	2.45	2.45
d(O_w...O_w)		2.74				2.73			

[a] Neutron diffraction experimental data (Gournis et al., 2008).
[b] Optimized at variable volume.
[c] Averaged values from MD simulations at 273 K and 40 bar.
[d] Averaged values from MD simulations at 320 K and 40 bar.

system at equilibrium, the particles will move in accordance with the equations of motion that define the system and, in general, will tend to diffuse away from their original location. For a stable crystal, the constituent atoms vibrate around their sites in the crystal lattice without diffusing. MSD profiles of H_2O molecules in the CO_2 and CO_2–CH_4 hydrates were calculated. MD simulations at stable conditions (Fig. 3) show a typical solid profile without diffusion, while under unstable conditions the collapse

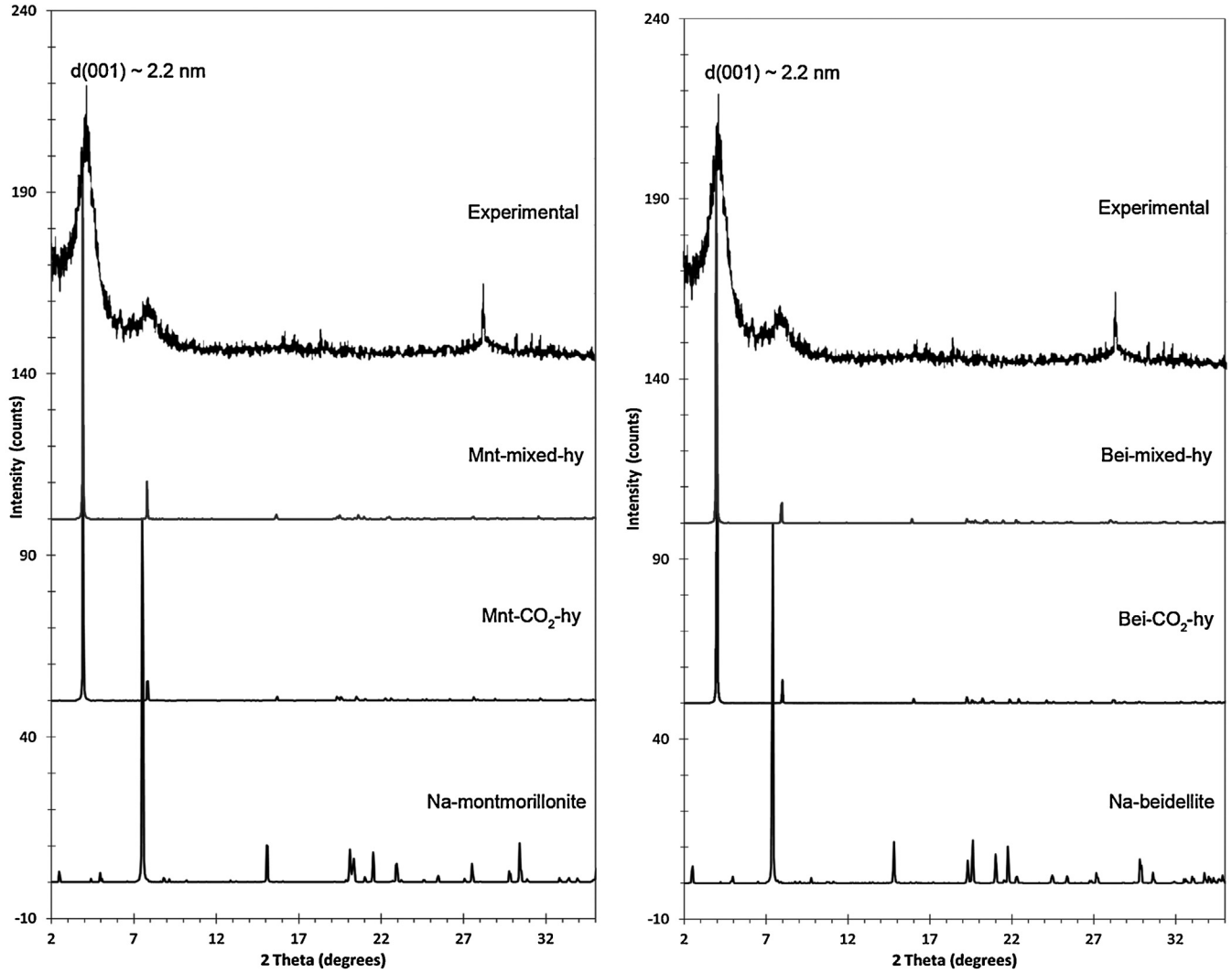

Fig. 4. Comparison of the experimental XRD pattern of montmorillonite-methane hydrate intercalate (Guggenheim and Koster van Groos, 2003 [28]) and simulated XRD patterns for the montmorillonite-CO_2 hydrate and montmorillonite-CH_4-CO_2 mixed hydrate (Mnt-CO_2-hy and Mnt-mixed-hy, left) and beidellite-hydrate intercalates (Bei-CO_2-hy and Bei-mixed-hy, right).

Table 3
Cell parameters and select interatomic spacings of the mixed CO_2–CH_4 hydrate (Hy) intercalates of Na-montmorillonite (Mnt) and Na-beidellite (Bei) unit cell (distances in Å and angles in°).

Features	Mnt-mixed-Hy[a]	S-Mnt-mixed-Hy[b]	U-Mnt-mixed-Hy[c]	Bei-mixed-Hy[a]	S-Bei-mixed-Hy[b]	U-Bei-mixed-Hy[c]
a	5.40	5.41	5.41	5.42	5.42	5.43
b	8.92	8.92	8.93	8.91	8.92	8.93
c	23.20	23.21	23.23	23.15	23.16	23.17
d(0 0 1)	22.76	22.76	22.74	22.36	22.36	22.35
α	93.9	93.9	93.9	90.3	90.3	90.3
β	101.7	101.7	101.7	105.4	105.4	105.4
γ	89.4	89.4	89.4	89.5	89.4	89.4
d(Si–O)	1.65	1.65	1.65	1.66	1.65	1.65
d(Al–O)	1.95	1.95	1.95	1.94	1.95	1.95
d(O–H)	0.95	0.95	0.95	0.94	0.95	0.95
d(Na…O_{clay})	2.40	2.40	2.40	2.35	2.35	2.35
d(Na…O_w)	2.45	2.45	2.45	2.44	2.45	2.45

[a] Optimized at variable volume.
[b] Averaged values from MD simulations at 273 K and 40 bar.
[c] Averaged values from MD simulations at 320 K and 40 bar.

of the crystal structure facilitates that the H_2O molecule diffusion occurs dramatically. Based on MSD profiles, the water diffusion coefficients were calculated, yielding 0.108 $Å^2\ s^{-1}$ for U-CO_2-Hy; 0.083 $Å^2\ s^{-1}$ for U-CH_4-CO_2-Hy; 4.5×10^{-4} $Å^2\ s^{-1}$ for S-CO_2-Hy, and 5×10^{-5} $Å^2\ s^{-1}$ for S-CH_4-CO_2-Hy. These results indicate that for the conditions studied, mixed CH_4—CO_2 hydrates are more stable than CO_2 hydrates. Comparing with previous MD simulations of methane hydrate [51] (Martos-Villa et al., 2013a) in the same conditions, we found that for the stable conditions, methane hydrate yields water diffusion coefficients even lower (5×10^{-6} $Å^2\ s^{-1}$).

4.2. Na-montmorillonite and Na-beidellite structures

Geometry optimizations of Na-montmorillonite and Na-beidellite models were performed at constant and variable volumes. The lattice parameters and the main geometrical features are consistent with experimental values (Table 2). MD simulations were performed at ambient conditions (298.15 K and 1 atm) for 50 ps. The MD simulations show that both models remain stable during the analysis. The mean basal *d*(0 0 1) value for Na-montmorillonite is 12.08 Å, and 12.34 Å for Na-beidellite. This swelling is in agreement with experiment [54,55] and with previous molecular simulations studies [56]. The Na…O (Table 2) distances indicate the coordination of Na with the water oxygens and the basal tetrahedral O atoms. These distances show that the Na ion is partly coordinated with the O_{clay} species. In beidellite, this distance is shorter owing to the $^{IV}Al^{3+}$ which generates a high charge excess in the basal O atoms and thus the coulombic interactions with Na are stronger. The values of O_{water}–O_{water} distances are close to experimental neutron diffraction data for liquid water [57].

4.3. Mixed CH_4—CO_2 hydrate intercalates

4.3.1. Geometry

The hydrate complexes of CO_2 and mixed CH_4—CO_2 intercalated in montmorillonite (Mnt-CO_2-Hy and Mnt-mixed-Hy) and in beidellite (Bei-CO_2-Hy and Bei-mixed-Hy) were optimized at constant and variable volume. XRD patterns of the optimized models were simulated (Fig. 4), obtaining a *d*(0 0 1) value close to 2 nm, in agreement with experimental results obtained by Guggenheim and Koster van Groos (2003) [28]. Geometry optimization at variable volume of the intercalated structures produced lattice parameters close to the experimental with an expanded "*c*" value of 23.24 Å in Mnt-CO_2-Hy, 23.20 Å in Mnt-mixed-Hy, 23.06 Å in Bei-CO_2-Hy, and 23.15 Å in Bei-mixed-Hy (Tables 2 and 3). No significant geometrical differences were found between Mnt-CO_2-Hy and Mnt-mixed-Hy. The beidellite intercalates have a slightly smaller interlayer thickness and smaller Na–O_{clay} distances than in montmorillonite owing to the tetrahedral charge of beidellite. This charge produces stronger interactions of the basal tetrahedral O atoms with Na cations and H atoms of water molecules. In all cases, the *d*(Na–O_{clay}) and *d*(Na–O_{water}) distances are similar, indicating that the Na cations are coordinated with the tetrahedral basal oxygens and the oxygens of the surrounding water molecules.

4.3.2. Adsorption energies

In this section the adsorption of gas hydrate in the interlayer of montmorillonite and beidellite models optimized at constant volume are considered. The adsorption energy calculated with CVFFH of mixed CO_2–CH_4 hydrate at montmorillonite surface is −32.81 kcal mol^{-1} per unit cell, whereas in beidellite the adsorption energy is −28.42 kcal mol^{-1}. The adsorption energy of CO_2 hydrate in montmorillonite surface is −32.43 kcal mol^{-1} per unit cell, whereas in beidellite the adsorption energy is −23.51 kcal mol^{-1}. Adsorption energy is more negative in the montmorillonite-hydrate complexes than in beidellite ones, which indicates that the montmorillonite-hydrate complexes are more stable. These differences in energy are related to the location of the layer charge in the clay mineral. Furthermore, adsorption energy of smectite-mixed CO_2–CH_4 hydrate complexes are slightly more negative than smectite-CO_2 hydrate complexes, indicating that the crystal structure of the mixed CO_2–CH_4 hydrate intercalated on smectites is slightly more stable than in the CO_2 hydrate intercalate.

4.3.3. Molecular Dynamics simulations

MD simulations were performed for 50 ps at different conditions for montmorillonite and beidellite hydrate intercalates: Simulations involve stable conditions at $P = 40$ bar and $T = 273$ K (S-Mnt-CO_2-Hy, S-Mnt-mixed-Hy, S-Bei-CO_2-Hy and S-Bei-mixed-Hy), and in unstable conditions at $P = 40$ bar and $T = 320$ K (U-Mnt-CO_2-Hy, U-Mnt-mixed-Hy, U-Bei-CO_2-Hy and U-Bei-mixed-Hy). In both minerals, the behavior of intercalates is similar. In the final configurations at the end of the MD simulations at stable conditions of the S-Mnt-Hy and S-Bei-Hy models, the water molecules are slightly disordered although the methane molecules remain in their initial positions.

Cell parameters were monitored during the simulations. Tables 2 and 3 show that the models remained stable after each simulation with cell parameters and bond distances close to the original Na-smectites. Each simulation showed a *d*(0 0 1) value close to the 2 nm characteristic peak for smectite-methane-hydrate intercalates. In Mnt-CO_2 hydrates, the *d*(Na–O_{clay}) distances are

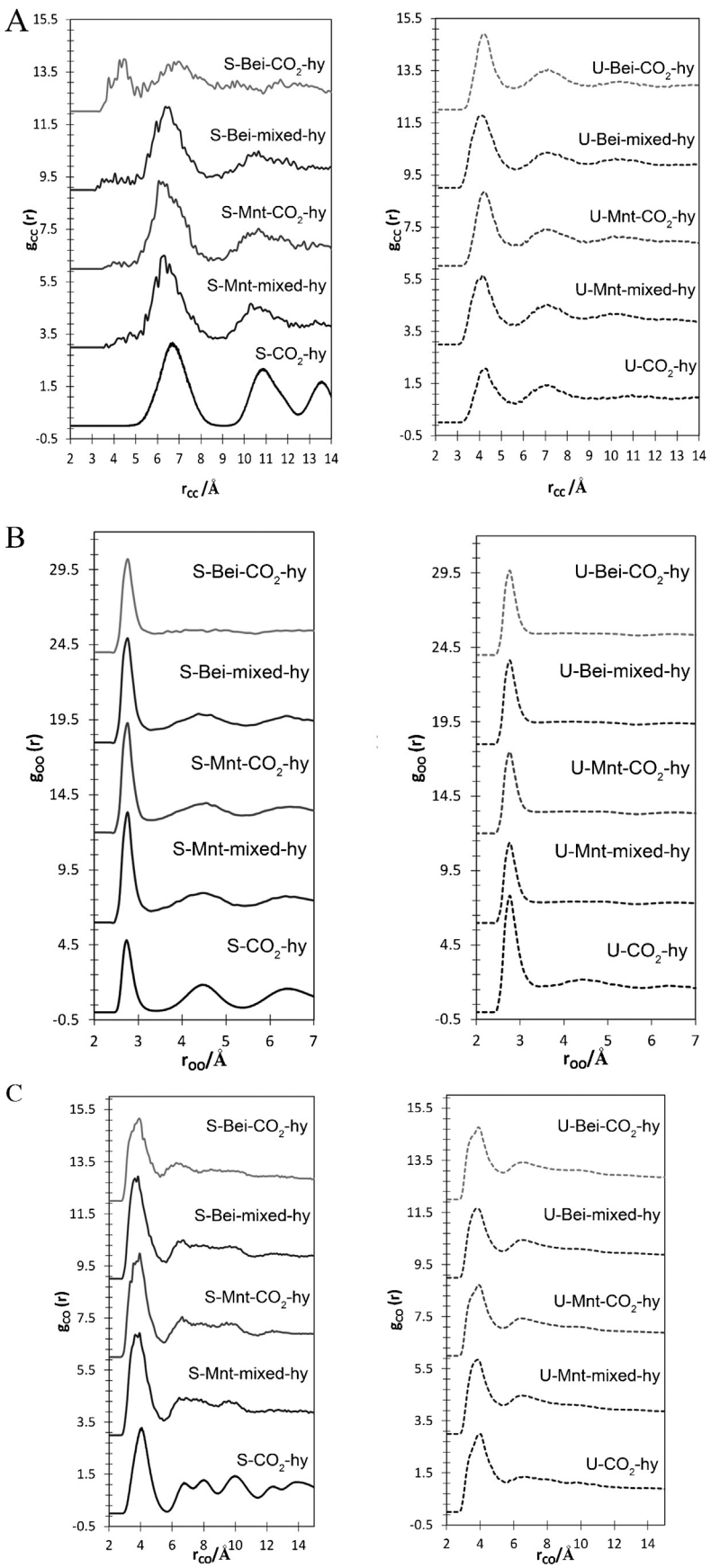

Fig. 5. RDFs of CC (a), OO (b), and CO (c), atoms of smectite-gas hydrate intercalates obtained from MD simulations and comparing with CO_2 hydrate crystal structure. Left, stable configurations (S-) obtained from MD at 273 K and 40 bar, right unstable configurations (U-) obtained from MD at 320 K and 40 bar.

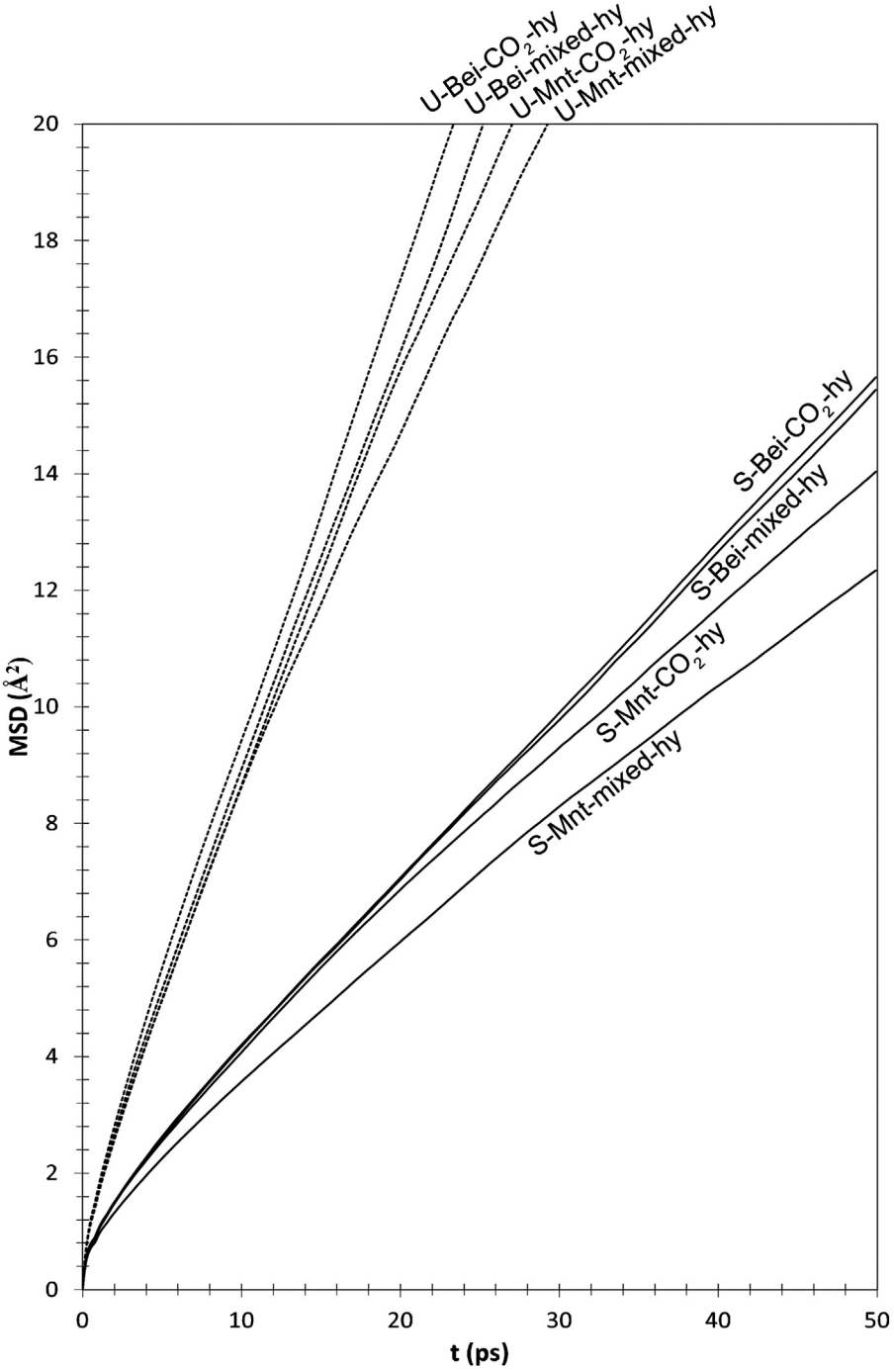

Fig. 6. MSD of water molecules in smectite-CO_2 and CH_4—CO_2 mixed hydrate intercalates obtained from MD simulations.

slightly longer in the MD simulated models than in the geometry optimized models.

The results of the MD simulations were analyzed by the RDF of C–C, C–O and O–O atom pairs taken from 1000 configurations sampled each 100 fs of the simulations. The atom-pair peaks were compared to previous results obtained by MD of the carbon dioxide hydrate model under stable and unstable conditions (S-CO_2-hy and U-CO_2-hy) (Fig. 5). The RDF peaks of C atoms in guest molecules, g_{C-C}, appear at r_{C-C} = 6.6 and 10.8 Å (Fig. 5a). These peaks are intense in the stable smectite-hydrate complexes, and they are coincident with S-CO_2-Hy peaks. However, in unstable smectite-hydrate complexes, the RDF profiles are clearly different and the most intense peak can be observed at closer C–C distances (3.9 Å) than in the hydrate, like in the CO_2 hydrates without smectite, and the rest of the peaks are drastically broader and with low intensity than in stable conditions, indicating that the crystal structure of hydrates has been decomposed segregating the guest molecules. In the simulations at stable conditions, there are small differences in the intensities of those peaks, being broader than without smectite owing to the certain disorder of the guest molecules. Nevertheless, the peaks are sharper in montmorillonite models than in beidellite, indicating that the structure of hydrates is more ordered in montmorillonite than in beidellite. Furthermore, a peak at 3.9 Å can be observed in the S-Bei-CO_2 hydrate model, indicating that

this beidellite-CO_2 hydrate complex is less stable than the montmorillonite one.

RDF profiles of O–O atom-pairs, g_{O-O}, display a common maximal peak at $r_{O-O} = 2.8$ Å, corresponding to the nearest distance between H_2O molecules linked by hydrogen bonds (Fig. 5b). This peak remains in all samples and all conditions. The second and third maximal peaks appearing in the CO_2 hydrate model at $r_{OO} = 4.6$ Å and 6.5 Å respectively, are well represented in the smectite-hydrate models determined under stable conditions, while in the beidellite-CO_2 hydrate model cannot be distinguished. In unstable conditions, these peaks are not observed showing the disorder structure of the water network and, then, the decomposition of the hydrate crystal. Those peaks correspond to oxygen coordination in hydrates and they only appear in O–O RDF profiles that includes the basal oxygen atoms. This result indicates that guest molecules close to 2:1 layer surface, are in sites formed by basal oxygen atoms and water molecules. These sites are also observed in RDF profiles of C and O atoms g_{C-O}, where a maximal peak at $r_{C-O} = 4$ Å occurs for all MD simulations (Fig. 5c). This peak corresponds to water molecules surrounding the guest molecules. However, the remaining peaks at 6.6 Å, 8.0 Å, and 9.8 Å of the hydrate model remain only in the stable conditions.

Fig. 6 illustrates the MSD profiles of H_2O molecules in the smectite-gas-hydrate intercalates. In the MD simulations under stable conditions, MSD profile shows a solid profile with low diffusion, whereas in the unstable structure the increase of temperature gives more freedom to atoms facilitating the diffusion of H_2O molecules. There are some differences between the montmorillonite and beidellite structures. In montmorillonite, MSD profiles show a lower diffusion of H_2O molecules than in beidellite, indicating that montmorillonite-gas hydrate intercalates are more stable than beidellite-gas-hydrate intercalates. Furthermore, there are differences in the type of hydrate intercalated in the smectites, where smectite-mixed CO_2–CH_4 hydrate intercalates are more stable than CO_2 hydrate intercalates. Based on MSD profiles, diffusion coefficients were calculated, yielding 0.038 $Å^2\ s^{-1}$ for S-Mnt-mixed-Hy; 0.043 $Å^2\ s^{-1}$ S-Mnt-CO_2-Hy; 0.048 $Å^2\ s^{-1}$ for S-Bei-mixed-Hy and 0.049 $Å^2\ s^{-1}$ for S-Bei-CO_2-Hy.

5. Conclusions

Crystalline structure of CO_2 and mixed hydrates can be successfully reproduced using computational methods based on DFT and using empirical interatomic potentials (CVFFH). Calculated binding energies of gas molecules into the hydrate clathrate cages yield negative values, proving the exothermic nature of the hydrate formation. Those energies are more negative in mixed CO_2–CH_4 hydrates than in CO_2 hydrates. Molecular Dynamics simulations show that under conditions of stability, crystalline structure of gas hydrate remains, but rising temperature hydrate decomposes, disordering the hydrogen bonding network. MSD profiles of water molecules on CO_2 hydrates shows greater diffusion than mixed CO_2–CH_4 hydrates. This can be due to the rotation of CO_2 molecules inside the cages being attracted by hydrogen atoms of water molecules [58].

The simulations presented here are in agreement with experimental data that shows a significantly expanded interlayer [28]. Water molecules form a hydrogen bonding network that encloses gas molecules in cages in the interlayer, maintaining the ordered crystal structure. Those water molecules close to the siloxane surface form mixed cages that enclose gas molecules between basal oxygen atoms of the tetrahedral silicate rings and water molecules from the hydrogen bonding network (Fig. 7). Based on this coordination, we suggest that the smectite 2:1 layer surface must provide a stabilizing influence on the formation of gas hydrate complexes.

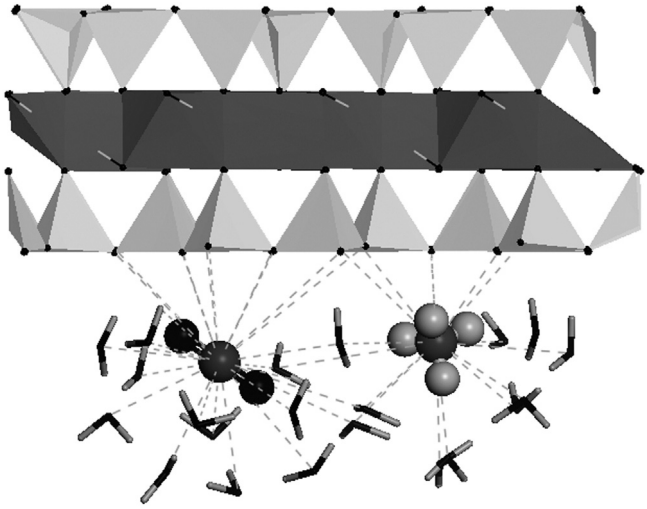

Fig. 7. Snapshot of mixed hydrate near a smectite surface. The gas molecules from clathrate cages are coordinated both water and clay surface oxygens. The carbon dioxide molecule (C in dark-gray and O in black ball), located in the center of a large cages is surrounded by water molecules; methane molecule (C in dark-gray ball and H in light-gray ball) are in small cages. Light-gray polygons represent Si atoms from tetrahedral smectite sheets; Dark-gray polygons represent Al atoms from octahedral smectite sheet.

Also, MSD calculations taken from MD simulations show that there are differences in the behavior of gas hydrate intercalates in montmorillonite vs beidellite models, where beidellite-gas hydrate complexes are less stable than montmorillonite-gas hydrate. Taking into account that, the difference between those two models is mainly the location of the layer charge in the smectite (octahedral charge in montmorillonite, tetrahedral charge in beidellite), this may be the determining factor in the stability of smectite-gas-hydrate intercalates. This result is also supported by the calculated adsorption energies, which are higher in the montmorillonite-gas hydrate complexes than in beidellite complexes. Furthermore, MSD and adsorption energies support that smectite-mixed CO_2–CH_4 hydrates intercalates are more stable than smectite-CO_2 complexes. Comparing with previous simulations on smectite-methane hydrate complexes [59], smectite-methane hydrate complexes are more stable than smectite-CO_2–CH_4 mixed and CO_2 hydrate complexes. Nevertheless, the difference in the adsorption energy between both kind of hydrates is not very large and also we are considering this stability as a fully ordered crystal structure. Therefore we can accept the existence of a partially disordered poorly crystalline hydrate structure in the interlayer of these minerals for both kinds of hydrates. Besides, taking into account the high disorder degree of the layers and cation substitution we have to develop analytical techniques to identify and characterize these poorly ordered complexes. This should be taken in account for CO_2 sequestration processes in hydrate reservoirs were smectites are present and as a caprock of the hydrate reservoir in the geological formations.

Injecting CO_2 into subsurface CH_4 hydrate reservoirs would displace some of the CH_4 in the hydrate crystal lattice, converting simple CH_4 hydrates into either simple CO_2 hydrates or double mixed CH_4—CO_2 hydrates. Our simulations prove that this conversion is also possible within the interlayer of swelling smectites, and that the type of clay influence the stability of the smectite-hydrate complexes, being more feasible to form those complexes on octahedrally charged smectites like montmorillonite than in tetrahedrally charged like beidellite.

Acknowledgements

Funding for this work came from Junta de Andalucía RNM-3581 CADHYS project and University of Cádiz doctoral scholarship. Authors are thankful to H. Heinz for his useful discussions and for facilitating the force fields, to W. Kuhs for the availability of crystal atomic data of methane hydrate, and to PAIDI-groups RNM-328 and RNM-363 of the Andalusian Government for the financial support, to the Supercomputational Center of the Granada University (UGRGRID), and the Centro Técnico de Informática of CSIC.

References

[1] K.A. Kvenvolden, Geol. Soc. Lond. Spec. Publ. 137 (1998) 9.
[2] B.A. Buffet, Annu. Rev. Earth Planet. Sci. 28 (2000) 477.
[3] A.V. Milkov, Org. Geochem. 36 (2005) 681.
[4] B.A. Buffet, D. Archer, Earth Planet. Sci. 227 (2004) 185.
[5] E. Burwicz, L.H. Rupke, K. Wallmann, Geochim. Cosmoquim. Acta 75 (2001) 4562.
[6] K. Wallmann, E. Piñero, E. Burwicz, M. Haeckel, C. Hensen, A. Dale, L. Ruepke, Energies 5 (2012) 2449.
[7] E. Piñero, M. Marquardt, C. Hensen, M. Haeckel, K. Wallmann, Biogeosciences 10 (2013) 959.
[8] G.J. Moridis, T.S. Collet, R. Boswell, S. Hancock, J. Rutqvist, C. Santamarina, T. Kneafseay, M.T. Reagan, M. Pooladi-Darvish, M. Kowalsky, E.D. Sloan, C. Coh, Adv. Biofuels Bioprod. 37 (2013) 977.
[9] K.A. Kvenvolden, B.W. Rogers, Mar. Petrol. Geol. 22 (2005) 579.
[10] C.A. Rochelle, A.P. Camps, D. Long, A. Milodowski, K. Baterman, D. Gunn, P. Jackson, M.A. Lovell, J. Rees, Geol. Soc. Lond. Spec. Publ. 319 (2009) 171.
[11] M. Ota, K. Morohashi, Y. Abe, M. Watanabe, R.L. Smith, H. Inomata, Energy Convers. Manage. 46 (2005) 1680.
[12] Y. Park, D.-Y. Kim, J.-W. Lee, D.-G. Huh, K.-P. Park, J. Lee, H. Lee, Proc. Natl. Acad. Sci. 103 (2006) 12690.
[13] Q. Zhou, X. Lu, X. Liu, L. Zhang, H. He, J. Zhu, P. Yuan, J. Colloid Interface Sci. 355 (2011) 237.
[14] B.J. Anderson, J.W. Tester, G.P. Borghi, B.L. Trout, J. Am. Chem. Soc. 125 (2005) 17852.
[15] N. Goel, J. Petrol. Sci. Eng. 51 (2006) 169.
[16] K. Ohgaki, K. Takano, H. Sangawa, T. Matsubara, S. Nakano, J. Chem. Eng. Jpn. 29 (1996) 478.
[17] R. Radhakrishnan, B.L. Trouta, J. Chem. Phys. 117 (2002) 1786.
[18] M. Ota, M. Ferdows, JSME Int. J. B 48 (2005) 802.
[19] A.A. Chialvo, M. Houssa, P.T. Cummings, J. Phys. Chem. B 106 (2002) 442.
[20] S. Hirai, K. Okazaki, Y. Tabe, K. Kawamura, Energy Convers. Manage. 38 (1997) S301.
[21] Y.-T. Tung, J.-L. Chen, Y.-P. Chen, S.-T. Lin, J. Phys. Chem. C 115 (2011) 7504.
[22] S. Sarupria, P.G. Debenedetti, J. Phys. Chem. A 115 (2011) 6102.
[23] J. Liu, J. Zhao, J. Xu, Comput. Theor. Chem. 991 (2012) 165.
[24] C. Geng, H. Wen, H. Zhou, J. Phys. Chem. 113 (2009) 5463.
[25] Y.X. Qi, M. Ota, H. Zhang, Energy Convers. Manage. 52 (2011) 2682.
[26] M.B. Clennell, M. Hovland, J.S. Booth, P. Henry, W.J. Winters, J. Geophys. Res. 104 (1999) 22985.
[27] T.F. Ertefai, V.B. Heuer, J. Prieto-Mollar, C. Vogt, S.P. Sylva, J. Seewald, K. Hinrichs, Geochim. Cosmochim. Acta 74 (2010) 6033.
[28] S. Guggenheim, A.F. Koster van Groos, Geology 31 (2003) 653.
[29] A. Busch, S. Alles, Y. Genterblum, D. Prinz, D.N. Dewhurst, M.D. Raven, H. Stanjek, B.M. Krooss, Int. J. Green. Gas Con. 2 (2008) 297.
[30] J. Wollenweber, S. Alles, A. Busch, B.M. Krooss, H. Stanjek, R. Litke, Int. J. Green. Gas Con. 4 (2010) 231.
[31] P. Giesting, S. Guggenheim, A.F. Koster van Groos, A. Busch, Int. J. Green. Gas Con. 8 (2012) 73.
[32] J.M. Soler, E. Artacho, J.D. Gale, A. García, J. Junquera, P. Ordejón, D. Sánchez-Portal, J. Phys. Condens. Mater. 14 (2002) 2745.
[33] B. Hammer, L.B. Hansen, J.K. Norskov, Phys. Rev. B 59 (1999) 7413.
[34] N. Troullier, J.L. Martins, Phys. Rev. B 43 (1991) 1993.
[35] A. Hernández-Laguna, E. Escamilla-Roa, V. Timón, M.T. Dove, C.I. Sainz-Díaz, Phys. Chem. Miner. 33 (2006) 655.
[36] C.I. Sainz-Díaz, E. Escamilla-Roa, A. Hernández-Laguna, Am. Mineral. 90 (2005) 1827.
[37] M.V. Fernández-Serra, E. Artacho, J. Chem. Phys. 121 (2004) 11136.
[38] Y. Liu, J. Zhao, F. Li, Chen, Z. J. Comput. Chem. 34 (2013) 121.
[39] L. Tang, Y. Su, Y. Liu, J. Zhao, R. Qiu, J. Chem. Phys. 136 (2012) 224508.
[40] H. Heinz, R.A. Vaia, L. Farmer, J. Chem. Phys. 124 (2006) 224713.
[41] C.I. Sainz-Díaz, M. Francisco-Márquez, A. Vivier-Bunge, Environ. Chem. 8 (2011) 429.
[42] B.H. Besler, K.M. Merz, P.A. Kollman, J. Comp. Chem. 11 (1990) 431.
[43] H.C. Andersen, J. Chem. Phys. 72 (1980) 9173.
[44] H.J.C. Berendsen, J.P.M. Postma, W.F.M. van Gusteren, A. DiNola, J.R. Haak, J. Chem. Phys. 37 (1984) 185.
[45] Materials Studio, Version 5.0, Accelrys Software, Inc., San Diego, CA, 2009.
[46] M.E. Molina-Montes, D. Donadio, C.I. Sainz-Díaz, A. Hernández-Laguna, M. Parrinello, J. Phys. Chem. B 112 (2008) 7051.
[47] J. Lee, S. Guggenheim, Am. Mineral. 66 (1981) 350.
[48] C.I. Sainz-Díaz, E.J. Palin, A. Hernández-Laguna, M.T. Dove, Phys. Chem. Miner. 30 (2003) 382.
[49] E.J. Palin, M.T. Dove, A. Hernández-Laguna, C.I. Sainz-Díaz, Am. Mineral. 89 (2004) 164.
[50] A. Klapproth, Ph.D. thesis, Georg-August-Universitat, Gottingen, Germany, 2002.
[51] R. Martos-Villa, M. Francisco-Márquez, M.P. Mata, C.I. Sainz-Díaz, J. Mol. Graph. Model. 44 (2013) 253.
[52] A.F. Koster van Groos, S. Guggenheim, Am. Mineral. 94 (2009) 372.
[53] K.A. Udachin, C.I. Ratcliffe, J.A. Ripmeester, J. Phys. Chem. B 105 (2001) 4200.
[54] A.M. Posner, J.P. Quirk, J. Colloid Sci. 19 (1984) 798.
[55] M.H. Fu, Z.Z. Zhang, P.F. Low, Clay Clay Miner. 38 (1999) 485.
[56] R.T. Cygan, S. Guggenheim, A.F. Koster van Groos, J. Phys. Chem. B 108 (2004) 15141.
[57] A.K. Soper, Chem. Phys. 258 (2000) 121.
[58] H. Jiang, K.D. Jordan, J. Phys. Chem. C 114 (2000) 5555.
[59] R. Martos-Villa, R.S. Guggenheim, M.P. Mata, C.I. Sainz-Díaz, F. Nieto, Am. Miner. (2014), in press.